






High-Bandwidth Arbitrary Signal Detection Using Low-Speed Electronics

Janosch Meier , Karanveer Singh, Arijit Misra , *Graduate Student Member, IEEE*, Stefan Preußler , J. Christoph Scheytt , *Member, IEEE*, and Thomas Schneider 

Abstract—The growing demand for bandwidth and energy efficiency requires new solutions for signal detection and processing. We demonstrate a concept for high-bandwidth signal detection with low-speed photodetectors and electronics. The method is based on the parallel optical sampling of a high-bandwidth signal with sinc-pulse sequences provided by a Mach-Zehnder modulator. For the electronic detection and processing this parallel sampling enables to divide the high-bandwidth optical signal with the bandwidth B into N electrical signals with the baseband bandwidth of $B/(2N)$. In proof-of-concept experiments with $N = 3$, we present the detection of 24 GHz optical signals by detectors with a bandwidth of only 4 GHz. For ideal components, the sampling and bandwidth down-conversion does not add an excess error to the signals and even for the non-ideal components of our proof-of-concept setup, it is below 1%. Thus, the rms error for the measurement of the 24 GHz signal was reduced by a factor of about 3.4 and the effective number of bits were increased by 1.8.

Index Terms—Analog-to-digital conversion, integrated photonics, optical sampling, optical signal processing.

I. INTRODUCTION

HIGH-bandwidth signal detection, processing and analysis has attracted much attention in recent years, since the data rates in the worldwide communication systems have increased drastically and a further growth is expected for the future [1], [2]. Additionally, the detection of ultra-short events in science and technology as well as in Radar, Lidar and security applications require the measurement of high-bandwidth signals [3].

Today high-bandwidth signal measurement is mainly based on a vast digital signal processing. With increasing bandwidths of the signals, the energy consumption growth. Additionally, nonlinearities and jitter problems in the detector lead to an

Manuscript received December 1, 2021; revised January 24, 2022; accepted February 2, 2022. Date of publication February 8, 2022; date of current version February 21, 2022. This work was supported in part by Deutsche Forschungsgemeinschaft (DFG, German Research Foundation) under Grants 424608109, 424608271, 424607946, 424608191, 403154102, and 322402243, and in part by the German Federal Ministry of Education and Research (BMBF, Bundesministerium für Bildung und Forschung) under Grant 13N14879. (Janosch Meier and Karanveer Singh contributed equally to this work.) (Corresponding author: Janosch Meier.)

Janosch Meier, Karanveer Singh, Arijit Misra, Stefan Preußler, and Thomas Schneider are with THz Photonics Group, Technische Universität Braunschweig, 38106 Braunschweig, Germany (e-mail: janosch.meier@ihf.tu-bs.de; karanveer.singh@ihf.tu-bs.de; arijit.misra@ihf.tu-bs.de; stefan.preussler@ihf.tu-bs.de; thomas.schneider@ihf.tu-bs.de).

J. Christoph Scheytt is with Research Group System and Circuit Technology, Universität Paderborn, 33102 Paderborn, Germany (e-mail: cscheytt@hni.upb.de).

Digital Object Identifier 10.1109/JPHOT.2022.3149389

TABLE I
COMPARISON TABLE WITH KEY PARAMETERS FOR DIFFERENT ADC SYSTEMS (BW = BANDWIDTH)

Method	BW	Sampl. Rate	ENOB
Int. time-interl. el. ADC [9]	31.5 GHz	56 GS/s	5.7
Int. time-interl. el. ADC [10]	13.3 GHz	28 GS/s	5.4
Opt. dual-freq. comb ADC [11]	12.5 GHz	–	4.5
Int. opt. ADC with MLL [12]	10 GHz	2.1 GS/s	3.5
This work	12 GHz	24 GS/s	5.9

increase of the measurement error and a decrease of the effective number of bits (ENOB) for higher signal bandwidths. Most of today's signal detection and measurement systems process digital data. Therefore, the first step of the digital signal processing is a sampling followed by an analog-to-digital conversion (ADC). The sampling rate and the connected signal bandwidth of the ADC define the maximum bandwidth of the signal that can be measured. In general, for high-bandwidth signal measurement different kinds of sampling techniques based on electrical samplers as electrical sample-and-hold circuits or optical samplers have been proposed [4]–[6]. The clock jitter of the electronic devices affects the quality of the detected signals, leading to performance degradation at high bandwidths [7]. Furthermore, high-bandwidth sample-and-hold circuits are accompanied with an increased sampling error, which can somehow be compensated with electronic signal processing, leading to increased system complexity and power consumption for high-bandwidth signals.

The application of optical sampling methods can circumvent some of the restrictions of purely electrical sampling, for instance by sampling with low-jitter optical pulses from a mode-locked laser (MLL) [8]. But this requires a high-quality MLL. An overview about different kinds of ADC systems and their performance is shown in Table I. It can be seen, that there are integrated electrical samplers with bandwidths above 30 GHz having an ENOB of 5.7 at a sampling rate of 56 GS/s [9]. Please note that a direct comparison with our method is not possible, since the digitizer used for the proof-of-concept experiments had a limited resolution of only 4.1 for 12 GHz signals. However, with the presented method we were able to improve the ENOB of our ADC from 4.1 to 5.9. For higher-resolution electrical ADC like in [9], our method would be able to improve the ENOB as well. We demonstrate a new concept for high-bandwidth arbitrary signal measurement using optical sampling with sinc-pulse sequences, which can be directly applied to an optical high-bandwidth signal, since no additional electro-optic conversion is needed.

The method is based on time-interleaving. By theory and experimental demonstration with an integrated Mach-Zehnder modulator [13], we will show that the parallelized sampling of the high-bandwidth signal can be error-free for ideal components. Therefore, detectors with a lower bandwidth in each branch, can significantly reduce the measurement error. Furthermore, with an RF source (an oscillator) and a modulator of bandwidth $B/3$, already a sampling of signals with the optical bandwidth B can be realized, while the overall bandwidth of the sinc-pulse sequence and the maximum sampling rate corresponds to B (at least twice the baseband width). Different to other methods, our sampling realizes inherently an overall sampling rate fitting to the bandwidth requirement corresponding to the sampling theorem, in this case 24 GS/s with a 12 GHz baseband bandwidth limit.

II. SAMPLING CONCEPT

According to the sampling theorem, each bandwidth-limited signal can be seen as the superposition of time-shifted sinc pulses, weighted with the sampling points describing the signal completely. If the signal is bandwidth-limited to B in the optical domain and correspondingly to $B/2$ in the baseband, the time shift between the sampling points is $\Delta T = 1/B$ and consequently the required sampling rate, or minimum bandwidth, for the measurement of this signal is B .

Sinc pulses are unlimited in time and thus a mathematical construct. Therefore, we are using sinc-pulse sequences instead and we will show that an ideal sampling can be achieved by these sinc-pulse sequences, which are orthogonal to each other, if the next sequence is time shifted to the previous by ΔT . Therefore, with the presented method pulses with a bandwidth B can be used to sample a signal with the same bandwidth. If non-orthogonal pulses are used, like the kind of rectangular pulses of the sample and hold circuits for electrical sampling, the sampling pulses need a much higher bandwidth than the signal to sample to avoid a mutual influence between the sampling points, due to a limited roll-off of practically achievable pulse shapes.

As shown in Fig. 1, the basic idea of the proposed method is to split the high-bandwidth signal (Fig. 1(a)) into N branches and to sample the signal in each branch with a sinc-pulse sequence with the bandwidth B but, a repetition or sampling rate of only B/N (Fig. 1(b)). In the next step the signal is converted to the electrical domain with a resulting baseband bandwidth of $B/(2N)$. As we will show by theory and in proof-of-concept experiments, the original sampling points of the high-bandwidth signal are (for ideal components) perfectly preserved in the low-bandwidth signal. In the last step the sampling points of the original high-bandwidth signal are measured with low-bandwidth electronics in parallel and the original signal is reconstructed from the sampling points. Thereby, according to the Walden plot, a bandwidth reduction by the factor 10, for instance, can be associated with an increased ENOB of 3.3 [12].

It is clear that, if the ratio between the bandwidth of the single pulse and the repetition rate in a pulse train goes to infinity and jitter problems are neglected, ideal sampling is possible. A mode locked laser, with pulses of several THz and a repetition rate in

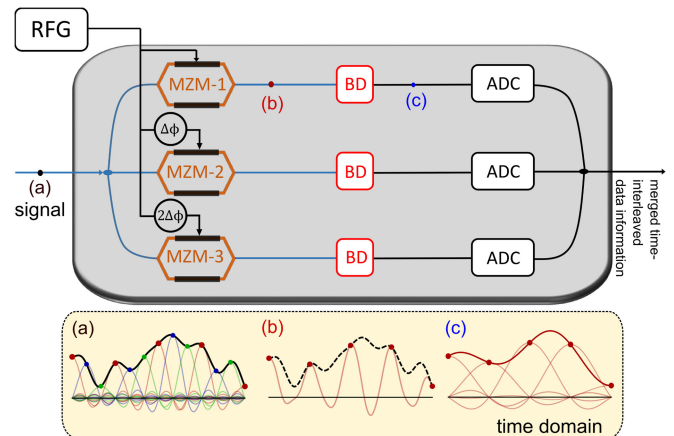


Fig. 1. Extraction of the sampling points for a three-branch system. The optical connections are drawn in blue, while the electrical connections are in black. For one sampling branch, the time domain representations of the signal are shown at the positions (a), (b), and (c) marked by the colored dots. (a) Represents the point, where the signal input is fed into the sampling system. (b) depicts the state after the pulse multiplication taking place inside the MZM and (c) shows the bandwidth-reduced waveform after the balanced detection with the preserved sampling points.

the MHz range comes close to this goal. In this case the single pulses of the pulse train are approaching a Dirac Delta. The same holds for a sinc-pulse train with a high number of N . If N goes to infinity, the single pulse of the train approaches an ideal sinc pulse.

However, here we will show that with our method ideal sampling is possible for each number of N and even for $N = 3$. In this case the sequence is far away from a sinc pulse and is in fact only a sinusoidal with a constant offset.

Thus, the presented method offers a bandwidth down-conversion of high-bandwidth signals without an additional error (for ideal components) and this can be achieved with very simple setups.

In the frequency domain, the multiplication of a signal with a sinc-pulse sequence corresponds to a convolution with a flat, finite frequency comb. Optical sinc-pulse sequences can be realized by spectral shaping of mode-locked lasers [14]. But this still needs an MLL along with optical filters. Furthermore, the optical filters are not rectangular and a nonlinear element is needed to realize the multiplication between the optical signal and the pulses [15]. A much easier way to generate high-quality sinc-pulse sequences is using one or two Mach-Zehnder Modulators (MZMs) [16]–[18]. The modulators are driven in the linear regime with a number of n sinusoidal frequencies and with changing their driving frequency, the repetition rate and bandwidth of the sequences can be easily adapted [19]. Such RF signals could be generated from a single integrated oscillator, which can be up-converted to very high frequencies delivering harmonics of the basic frequency [20]. For reaching high output powers as well as high frequencies, semiconductors, such as Indium Phosphide (InP) and Gallium Arsenide (GaAs), are suited to fabricate high-electron mobility transistors or heterojunction bipolar transistors, which can be combined with Schottky diodes to realize frequency multiplying chains. With this, transmission

powers of hundreds of mW at a few hundreds of GHz and up to a few mWs above 1 THz have been demonstrated for THz communication experiments [21], [22]. Finally, the optical pulse sequence can be shifted in time by a simple phase change of the used electrical driving signal [23]. The generation of the pulses has also been demonstrated on a silicon-photonics platform along with the sampling of pseudo random data signals by these pulses [24], [25]. If the driving signal is a multitone signal with frequencies of the same phases, one modulator driven by n equidistant frequencies can already produce a frequency comb with $N = 2n + 1$ lines [23]. These n lines can be the different harmonics generated by the up-conversion.

The quality and bandwidth of the modulator and the RF source define the performance of the ADC. For $N = 3$ just one ($n = 1$) single RF driving frequency is necessary and the required RF bandwidth of the MZM is $B/3$ and the jitter corresponds to that of the radio frequency generator (RFG) used for driving the modulator and is therefore defined by the repetition rate and not the bandwidth of the pulses [24], [26]. Thus, using this sampling principle, a high-bandwidth signal detection with a small jitter can be achieved, if a corresponding electrical source with a low jitter is used. With integrated low-jitter electrical RF sources, values in the femtosecond range can be reached [27]. But with more sophisticated RF sources, even atto- or zeptosecond jitters are possible [28], [29]. The system performance is limited by the signal-to noise ratio (SNR). An increase of the number of branches N results in a decrease of the bandwidth requirements in the single branch and theoretically the number of branches is not limited. However, this divides the power of the incoming signal in each branch at least by the factor N . Although, this can be compensated by amplifiers, it will result in a reduction of the SNR.

III. THEORY

According to the sampling theorem, the sampling points represent the full information of the signal and can be used to reconstruct the signal completely. Next, we will show that these sampling points are accurately preserved for ideal components in the bandwidth-reduced waveforms.

A single sinc pulse can be defined in the time domain as:

$$\text{sinc}(t) := \lim_{x \rightarrow t} \left(\frac{\sin(\pi x)}{\pi x} \right) \quad (1)$$

In the frequency domain this corresponds to the rectangular function $\Pi(f)$:

$$[\mathcal{F}_t(\text{sinc}(t))](f) = \Pi(f) \quad (2)$$

with \mathcal{F}_t as the Fourier transform operator and $\Pi(f) = 1$ for $|f| < 1/2$, $1/2$ for $|f| = 1/2$ and 0 elsewhere. Sinc pulses are infinite in time and as such as well only a mathematical construct, like Dirac Delta sequences. A sinc-pulse sequence, instead, with $N - 1$ zero crossings between two consecutive pulses and the bandwidth B , corresponds to an N -line rectangular comb in the frequency domain, which can easily be generated with an MZM, for instance. Sinc-pulse sequences can be seen as an infinite

superposition of sinc pulses [16], [30]. Such an infinite superposition is practically not possible as well. However, sequences with several tenths of GHz pulses running for hours or days can practically be seen as infinite. Sinc-pulse sequences can be expressed as:

$$\text{sq}_{N,B}(t) := \frac{2}{N} \left(\frac{1}{2} + \sum_{k=1}^{\frac{N-1}{2}} \cos\left(\frac{2\pi k B t}{N}\right) \right) \quad (3)$$

(3) is derived from the Fourier series. Thus, in the frequency domain the N -line comb can be written as:

$$\begin{aligned} [\mathcal{F}_t(\text{sq}_{N,B}(t))](f) &= \text{Comb}_{N,B}(f) := \sum_{k=-\frac{N-1}{2}}^{\frac{N-1}{2}} \frac{\delta(f - \frac{kB}{N})}{N} \\ &= \left(\sum_{k=-\infty}^{\infty} \frac{\delta(f - \frac{kB}{N})}{N} \right) \cdot \Pi\left(\frac{f}{B}\right) \end{aligned} \quad (4)$$

Therefore, the frequency representation of the sinc-pulse sequence is the multiplication between an infinite Dirac delta comb with a rectangular function, leading to a finite, rectangular frequency comb with N lines. Sampling is the multiplication of a signal $s(t)$ with the sampling function. Any signal $s(t)$ multiplied with a sinc-pulse sequence in the time domain is the convolution between its spectrum and a frequency comb. With an N -line sinc-pulse sequence, the periodicity of the sampling points is N/B . Similarly, with N time-interleaved N -line sinc-pulse sequences, the periodicity will be $1/B$. This characterizes a signal with baseband bandwidth $B/2$, which for the time signal $s(t)$ is given by:

$$s(t) = \sum_{m=-\infty}^{\infty} s\left(t_0 + \frac{m}{B}\right) \cdot \text{sinc}(Bt - Bt_0 - m) \quad (5)$$

Here t_0 denotes a temporal shift, which demonstrates, that the chosen sampling points can be shifted to any arbitrary time position.

After multiplication with the time-interleaved sinc-pulse sequence in the N branches, the sampling points of the signal are defined by the respective peak points of the used sinc-pulse sequence. These optical samples can be retrieved in each branch by a low bandwidth detector of the baseband bandwidth $B/(2N)$.

Since the theory guaranteeing the preservation of the sampling points is not simply based on the orthogonality of the sinc pulses or sinc-pulse sequences, the mathematical concept is described in detail in the following. The full sampling process in one branch, including the filtering with a rectangular filter, in the time domain at the sampling point $t_s = mN/B + \Delta t$ (with m as an integer) can be expressed as:

$$\begin{aligned} y(t_s) &= \left[\mathcal{F}_f^{-1} \left(\left[\mathcal{F}_t(s(t) \cdot \text{sq}_{N,B}(t - \Delta t)) \right](f) \cdot \Pi\left(\frac{Nf}{B}\right) \right) \right](t_s) \end{aligned} \quad (6)$$

where Δt corresponds to the time shift of the sinc-pulse sequence in the branch and \mathcal{F}_f^{-1} is the inverse Fourier transform operator.

By applying the convolution theorem, (6) can be expressed as:

$$y(t_s) = \left[\mathcal{F}_f^{-1} \left(\left[\mathcal{F}_t \left(s(t) \cdot \text{sinc}_{N,B}(t - \Delta t) \right) \right] (f) \right) \right] * \left[\mathcal{F}_f^{-1} \left(\Pi \left(\frac{Nf}{B} \right) \right) \right] (t_s) \quad (7)$$

By inserting the sampling points and applying symmetry and shifting properties of the sinc-pulse sequence, (7) can be further simplified to:

$$\begin{aligned} y(t_s) &= \int_{-\infty}^{\infty} s(t_s - \tau) \cdot \text{sinc}_{N,B}(t_s - \tau - \Delta t) \cdot \frac{B}{N} \cdot \text{sinc} \left(\frac{B\tau}{N} \right) d\tau \\ &= \int_{-\infty}^{\infty} s(t_s - \tau) \cdot \text{sinc}_{N,B}(\tau) \cdot \frac{B}{N} \cdot \text{sinc} \left(\frac{B\tau}{N} \right) d\tau \end{aligned} \quad (8)$$

With a multiplication theorem between sinc pulses and sinc-pulse sequences [31], it can be written:

$$y(t_s) = \int_{-\infty}^{\infty} s(t_s - \tau) \cdot \frac{B}{N} \cdot \text{sinc}(B\tau) d\tau \quad (9)$$

By using the forward and inverse Fourier transform, (9) becomes:

$$y(t_s) = \left[\mathcal{F}_f^{-1} \left(\left[\mathcal{F}_t \left(\int_{-\infty}^{\infty} s(t - \tau) \cdot \frac{B}{N} \cdot \text{sinc}(B\tau) d\tau \right) \right] (f) \right) \right] (t_s) \quad (10)$$

This can be used to apply the convolution theorem. By taking the Fourier transform of the sinc pulses, (10) changes to:

$$\begin{aligned} y(t_s) &= \frac{1}{N} \left[\mathcal{F}_f^{-1} \left(\left[\mathcal{F}_t(s(t)) \right] (f) \cdot \left[\mathcal{F}_t(B \cdot \text{sinc}(Bt)) \right] (f) \right) \right] (t_s) \\ &= \frac{1}{N} \left[\mathcal{F}_f^{-1} \left(\left[\mathcal{F}_t(s(t)) \right] (f) \cdot \Pi \left(\frac{f}{B} \right) \right) \right] (t_s) \end{aligned} \quad (11)$$

Here we use the fact that the bandwidth of the rectangular function corresponds to the maximum signal bandwidth and the forward and inverse Fourier transform will cancel each other. We note that the rectangular function in (11) is a result of the convolution between the rectangular frequency comb and the rectangular filter with a bandwidth of only $B/(2N)$. From (11), it follows:

$$y(t_s) = \frac{1}{N} s(t_s) \quad (12)$$

Thus, except a linear scaling factor $1/N$ the sampling points are preserved in the process. Therefore, the electrical signal with a reduced bandwidth of $B/(2N)$ detected in each of the N branches is different from the high-bandwidth input signal, but the sampling points taken with a periodicity N/B are the same as that in the original signal. So, this set of sampling points of the high-bandwidth signal can be measured by low-bandwidth equipment. That the sampling points are preserved accurately, is a specific property of the sinc-pulse sequences. For sampling with other types of pulse sequences, for example based on

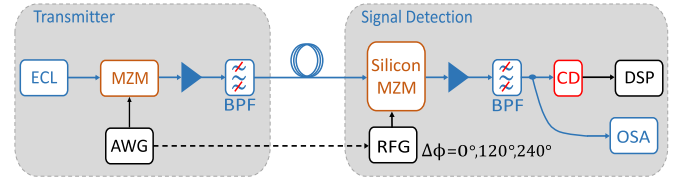


Fig. 2. Experimental setup for high-bandwidth signal detection using sampling by an integrated silicon Mach-Zehnder modulator (MZM). ECL; external cavity laser, AWG; arbitrary waveform generator, BPF; bandpass filter, RFG; radio frequency generator, CD; coherent detection, DSP; digital signal processing, OSA; optical spectrum analyzer.

Gaussian pulses, the proposed identity would be fulfilled only approximately leading to an inherent systematical error.

The whole set of sampling points will be finally measured with N branches. By inserting (12) into (5), the sampled signal $s(t)$ can be reconstructed from its sampling points by:

$$\begin{aligned} s(t) &= \sum_{m=-\infty}^{\infty} \sum_{k=1}^N \left[\mathcal{F}_f^{-1} \left(\left[\mathcal{F}_t \left(s(t) \cdot \text{sinc}_{N,B} \left(t - t_0 - \frac{k-1}{B} \right) \right) \right] (f) \right) \right. \\ &\quad \cdot \Pi \left(\frac{Nf}{B} \right) \left. \right] \left(t_0 + \frac{k-1}{B} + \frac{mN}{B} \right) \\ &\quad \cdot N \cdot \text{sinc}(Bt - Bt_0 - (k-1) - mN) \end{aligned} \quad (13)$$

Accordingly, a signal with an optical bandwidth up to B can be detected by electronics with a bandwidth of $B/(2N)$. Please note that this holds for any number of comb lines N .

In (6) we have assumed an ideal rectangular filter. Thus, there will be an error from the practical filter function. However, the required filter bandwidth is only $B/(2N)$ and it is practically much easier to get almost rectangular filter functions with low-bandwidth than with high-bandwidth electronics. Furthermore, for retrieving the sampling points still an electronic ADC is required and the jitter of the optical sinc-pulse sequence might as well lead to an error in the sampling process. However, the bandwidth requirements for the electronic ADC are reduced by N and the jitter for the sinc-pulse sequences corresponds to that of the RF source, with $1/3$ of the sampling rate for a three-line comb. Thus, even for non-ideal components, a signal detection with very high-quality should be possible, which we will show in the following proof-of-concept experiments.

IV. RESULTS

For high-bandwidth signal detection using the presented method, we have adapted the concept to its minimum complexity as shown in Fig. 2. A flat three-line frequency comb, corresponding to a sinc-pulse sequence with two zero crossings, is used to sample the incoming high-bandwidth signal. Achieving such a flat three-line frequency comb is very simple since it only requires the setting of bias and RF voltage of the MZM in a way that the carrier and sidebands have the same amplitude. Three branches with time-shifted sinc-pulse sequences are required to

extract the sampling points. However, due to a lack of equipment and for experimental simplicity, we have just realized one single branch and have measured the sampling points consecutively by a phase change of the electrical driving signal.

For sampling, we used an integrated MZM, fabricated using $0.25\ \mu\text{m}$ BiCMOS technology provided by IHP [13], which facilitates monolithic integration of photonic and electronic components on the same substrate. The high DC extinction ratio of 40 dB and a 3-dB bandwidth of 20 GHz makes it a suitable candidate for high-quality sinc-pulse sequence generation [25]. The sampled signals were detected by a coherent detector (CD) and its spectrum was monitored in parallel by an optical spectrum analyzer (OSA).

For the signal generation (transmitter), a 1550.1 nm wave is modulated by a LiNbO_3 MZM with an arbitrary waveform generator (AWG). For the sampling the on-chip silicon MZM is driven with a 10 GHz and 8 GHz sinusoidal signal respectively, generated by a radio frequency generator (RFG). The time shift of the sampling is adjusted by a proper phase shift of the RFG. The sampling points are extracted from the detector and the reconstruction is carried out by offline processing according to (13). A filter applied in the digital signal processing (DSP) stage reduces the bandwidth of the signal to $B/(2N)$. Erbium doped fiber amplifiers and bandpass filters are used to suppress the out of band amplified spontaneous emission noise and to compensate for the coupling losses of the chip.

For the first set of experiments, high-speed cosine waves are sampled by a three-line, flat comb with 10 GHz spacing in a single branch, resulting in a sampling rate of 10 GSa/s for the single and 30 GSa/s for all three branches. The results are demonstrated in Fig. 3. The blue line is the input waveform and the orange line is the measured result for one single branch. Thus, as expected, the sampled and detected waveform is a sinusoidal with a reduced bandwidth compared to the original signal. The black dashed line gives a theoretical fit to the signal from the extracted sampling points. Fig. 3(a) demonstrates the detection for a 6 GHz sine, leading to a 4 GHz sine in the detector. In Fig. 3(b), the detection of an 8 GHz sine leading to a 2 GHz sine is shown and Fig. 3(c) and (d) presents the detection of a 13 GHz sine leading to a 3 GHz sine and a 14 GHz sine leading to a 4 GHz sine, respectively.

By putting the information from all branches together, the sampling points for the full reconstruction of the signal can be extracted, which we have shown in Fig. 4 with an arbitrary signal reconstructed using the presented concept. Since in our proof-of-concept setup the sampling points were taken subsequently and not in parallel, we utilized a Nyquist data signal (pseudo random bit sequence), so that each sampling point belongs to a symbol point. This makes the reconstruction of the original high-bandwidth signal easier, since it gives a time reference between the measurements. The signal had 12 GHz baseband bandwidth and a symbol rate of 24 GBd in a rectangular optical bandwidth of 24 GHz. The symbol rate was limited by the available AWG. For the sampling a three-line comb sequence with a spacing of 8 GHz (24 GHz bandwidth) has been used. The detector bandwidth was restricted to $B/(2N) = 4\ \text{GHz}$ by an electronic setting of the DSP.

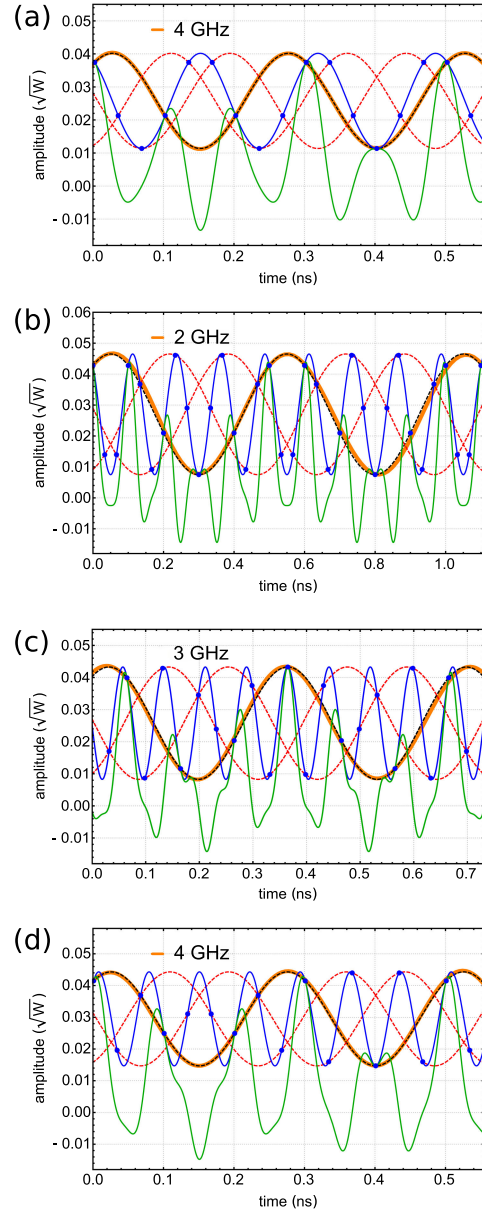


Fig. 3. Measurement of different sine waves using the presented method. The splitting of the high frequency sinusoidal (depicted in blue) into three sinusoids with reduced bandwidth is shown with the orange and the two red-dashed lines. The orange line is the sampled and detected result of one sampling branch. The fitting to the waveform from the extracted sampling points is shown with the black-dashed line. The green line shows the simulated pulse sequence. (a) 6 GHz sine, down-converted to a 4 GHz sine. (b) 8 GHz sine, down-converted to a 2 GHz sine. (c) 13 GHz sine, down-converted to a 3 GHz sine. (d) 14 GHz sine, down-converted to a 4 GHz sine.

The calculated rms error for the reconstructed signal, calculated as the maximum value minus the minimum value from the reference waveform (the signal applied to the AWG), was around 3.4% (Fig. 4). For a comparison, we have tried to measure the 24 GBd signal directly with the electrical equipment in a back-to-back configuration. Since the bandwidth of our detector is limited, this first attempt failed. We had to filter the signal (again in the DSP) by a 12 GHz raised cosine filter with a roll-off factor of 0.4 to get a trace out of the device. This measurement resulted in an rms error of 11.6% thus, 3.4 times higher.

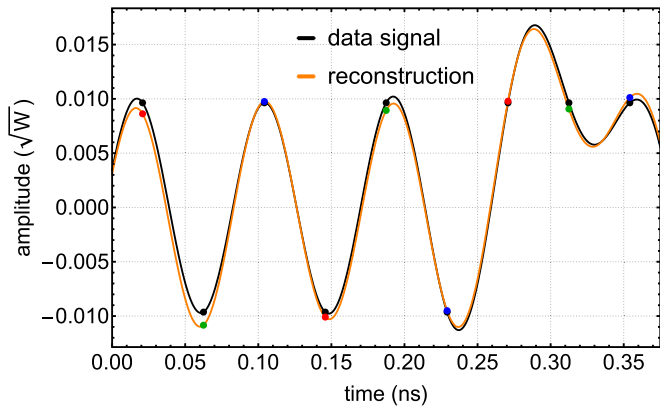


Fig. 4. Signal reconstruction of a two level data signal with a bandwidth of 24 GHz (24 GBd symbol rate) using a 4 GHz detector with the presented method. The original data signal and its sampling points are drawn in black. The reconstructed signal, based on the extracted sampling points from the low-bandwidth signals, is shown in orange. The sampling points from the three different branches (here measured consecutively) are shown in red, green and blue.

For a further comparison, the AWG and the detector were utilized in a back-to-back configuration to measure signals with a baseband bandwidth of 4 GHz and the measured rms error was around 2.9%. Therefore, the bandwidth splitting by our method had an excess error of less than one percent.

Based on the rms errors, we have made an estimation for the ENOB values using the following equation:

$$ENOB = \log_2(SINAD) - \log_2\left(\frac{2G \cdot A}{FSR}\right) - 0.292 \quad (14)$$

where $SINAD$ is the signal-to-noise-and-distortion ratio, G is the gain factor which we set as 1, A is the signal amplitude of the reference waveform and FSR is the full-scale range of the ADC [32]. In our case the $SINAD$ was given by:

$$SINAD = \frac{A}{\sqrt{2} \cdot NAD} = \frac{1}{\sqrt{2} \cdot 2RMS} \quad (15)$$

where NAD is the unnormalized rms noise and distortion in the time domain, and RMS is the normalized rms error. The additional factor 2 in front of the normalized rms error comes from the fact, that we have normalized the rms error by the the maximum value minus the minimum value. For the direct detection the ENOB is 4.1, whereas our method results in an ENOB of 5.9. Therefore, the estimated ENOB increment is with 1.8 a little bit higher than the 1.6, which can be expected, due to the bandwidth down-conversion from the Walden plot. Furthermore, we have conducted a simulation of an ENOB experiment with the software OptiSystem for a three-line frequency comb with 30 GHz bandwidth. In this simulation we achieved for the digitization of a 14.5 GHz sine wave an ENOB increment of 1.4 in comparison to the direct detection of the same waveform. Thereby the ENOB values of the digitizers were defined according to the Walden plot, so that our advantage was slightly smaller than 1.6 which could be theoretically expected. We address this difference to some remaining non-idealities of our simulation system.

V. CONCLUSION

In conclusion, we have proposed and experimentally demonstrated the detection of high-bandwidth signals with low-bandwidth detectors based on the bandwidth reduction of the signal enabled by sampling in a Mach-Zehnder modulator. For ideal components, the original sampling points are accurately preserved in the bandwidth reduced waveforms. However, even for non-ideal components an accurate measurement is possible. In proof-of-concept experiments we have shown the detection of up to 24 GHz signals by detectors with a bandwidth of only 4 GHz. The rms error for the measurement was reduced by a factor of 3.4, resulting in an increase in the ENOB of 1.8.

The method can be realized by any kind of MZMs. For a three-line comb the maximum sampling rate corresponds to three times the RF bandwidth of the modulator. Thus, for instance with 100 GHz modulators as shown in silicon photonics [33] already sampling rates of 300 GSa/s are possible in an integrated device and even higher modulator bandwidths have been demonstrated [34], [35]. In principle, other types of modulators providing flat frequency combs with linear phase dependent lines might as well be suited for a realization of the proposed sampling concept, whereby integrated ring modulators would be a very promising alternative due to their small footprint [36], [37].

ACKNOWLEDGMENT

The authors would like to thank Ranjan Das, Younus Mandalawi and Mohammed Hosni from TU Braunschweig for the constructive discussions.

REFERENCES

- [1] P. J. Winzer and D. T. Neilson, "From scaling disparities to integrated parallelism: A decathlon for a decade," *J. Lightw. Technol.*, vol. 35, no. 5, pp. 1099–1115, Mar. 2017.
- [2] P. J. Winzer, D. T. Neilson, and A. R. Chraplyvy, "Fiber-optic transmission and networking: The previous 20 and the next 20 years," *Opt. Exp.*, vol. 26, no. 18, pp. 24190–24239, Sep. 2018.
- [3] P. McManamon, "Review of ladar: A historic, yet emerging, sensor technology with rich phenomenology," *Opt. Eng.*, vol. 51, no. 6, pp. 1–14, 2012.
- [4] C. Schmidt-Langhorst and H.-G. Weber, "Optical sampling techniques," *J. Opt. Fiber. Commun. Rep.*, vol. 2, pp. 86–114, 2005.
- [5] S. Gupta and B. Jalali, "Time-warp correction and calibration in photonic time-stretch analog-to-digital converter," *Opt. Lett.*, vol. 33, no. 22, pp. 2674–2676, Nov. 2008.
- [6] C. Deakin and Z. Liu, "Dual frequency comb assisted analog-to-digital conversion," *Opt. Lett.*, vol. 45, no. 1, pp. 173–176, Jan. 2020.
- [7] D. Fang *et al.*, "320 GHz analog-to-digital converter exploiting Kerr soliton combs and photonic-electronic spectral stitching," in *Proc. Eur. Conf. Opt. Commun.*, 2021, pp. 1–4.
- [8] G. C. Valley, "Photonic analog-to-digital converters," *Opt. Exp.*, vol. 15, no. 5, pp. 1955–1982, Mar. 2007.
- [9] K. Sun, G. Wang, Q. Zhang, S. Elahmadi, and P. Gui, "A 56-GS/s 8-bit time-interleaved ADC with ENOB and BW enhancement techniques in 28-nm CMOS," *IEEE J. Solid-State Circuits*, vol. 54, no. 3, pp. 821–833, Mar. 2019.
- [10] M. Q. Le *et al.*, "A background calibrated 28GS/s 8b interleaved SAR ADC in 28 nm CMOS," in *Proc. IEEE Custom Integr. Circuits Conf.*, 2017, pp. 1–4.
- [11] C. Deakin, T. Odedeyi, and Z. Liu, "Dual frequency comb photonic analog to digital conversion," in *Proc. IEEE Photon. Soc. Summer Topicals Meeting Ser.*, 2020, pp. 1/2.
- [12] A. Khilo *et al.*, "Photonic ADC: Overcoming the bottleneck of electronic jitter," *Opt. Exp.*, vol. 20, no. 4, pp. 4454–4469, 2012.

- [13] C. Kress, K. Singh, T. Schwabe, S. Preußler, T. Schneider, and J. C. Scheytt, "High modulation efficiency segmented Mach-Zehnder modulator monolithically integrated with linear driver in 0.25 μm BiCMOS technology," in *Proc. Integr. Photon. Res., Silicon Nanophoton.*, Optical Society of America, 2021, Art. no. IW1B.1.
- [14] M. Nakazawa, T. Hirooka, P. Ruan, and P. Guan, "Ultrahigh-speed "orthogonal" TDM transmission with an optical Nyquist pulse train," *Opt. Exp.*, vol. 20, no. 2, pp. 1129–1140, Jan. 2012.
- [15] T. Hirooka, D. Seya, K. Harako, D. Suzuki, and M. Nakazawa, "Ultrafast Nyquist OTDM demultiplexing using optical Nyquist pulse sampling in an all-optical nonlinear switch," *Opt. Exp.*, vol. 23, no. 16, pp. 20858–20866, Aug. 2015.
- [16] M. A. Soto *et al.*, "Optical sinc-shaped Nyquist pulses of exceptional quality," *Nat. Commun.*, vol. 20, no. 1, pp. 1–11, 2013.
- [17] M. A. Soto *et al.*, "Generation of Nyquist sinc pulses using intensity modulators," in *Proc. Conf. Lasers Electro-Opt.*, 2013, pp. 1/2.
- [18] J. Hu, S. J. Fabbri, and C.-S. Brs, "Flexible width Nyquist pulse based on a single Mach-Zehnder modulator," in *Proc. Conf. Lasers Electro- Opt.*, 2018, pp. 1/2.
- [19] S. Preußler, N. Wenzel, and T. Schneider, "Flexible Nyquist pulse sequence generation with variable bandwidth and repetition rate," *IEEE Photon. J.*, vol. 6, no. 4, pp. 1–8, Aug. 2014.
- [20] I. Kallfass *et al.*, "All active MMIC-Based wireless communication at 220 GHz," *IEEE Trans. THz Sci. Technol.*, vol. 1, no. 2, pp. 477–487, Nov. 2011.
- [21] K. M. K. H. Leong *et al.*, "850 GHz receiver and transmitter front-ends using InP HEMT," *IEEE Trans. THz Sci. Technol.*, vol. 7, no. 4, pp. 466–475, Jul. 2017.
- [22] J. V. Siles, K. B. Cooper, C. Lee, R. H. Lin, G. Chattopadhyay, and I. Mehdi, "A new generation of room-temperature frequency-multiplied sources with up to $10\times$ higher output power in the 160-GHz–1.6-THz range," *IEEE Trans. THz Sci. Technol.*, vol. 8, no. 6, pp. 596–604, Nov. 2018.
- [23] J. Meier, A. Misra, S. Preußler, and T. Schneider, "Optical convolution with a rectangular frequency comb for almost ideal sampling," *Proc. SPIE*, G. Li and X. Zhou, Eds., 2019, vol. 10947, pp. 108–115.
- [24] S. Liu *et al.*, "Optical frequency comb and Nyquist pulse generation with integrated silicon modulators," *IEEE J. Sel. Top. Quantum Electron.*, vol. 26, no. 2, pp. 1–8, Mar./Apr. 2020.
- [25] A. Misra, C. Kress, K. Singh, S. Preußler, J. C. Scheytt, and T. Schneider, "Integrated source-free all optical sampling with a sampling rate of up to three times the RF bandwidth of silicon photonic MZM," *Opt. Exp.*, vol. 27, no. 21, pp. 29972–29984, Oct. 2019.
- [26] K. Singh, J. Meier, A. Misra, S. Preußler, J. C. Scheytt, and T. Schneider, "Photonic arbitrary waveform generation with three times the sampling rate of the modulator bandwidth," *IEEE Photon. Technol. Lett.*, vol. 32, no. 24, pp. 1544–1547, Dec. 2020.
- [27] M. Bahmanian, S. Fard, B. Koppelman, and J. C. Scheytt, "Wide-band frequency synthesizer with ultra-low phase noise using an optical clock source," in *Proc. IEEE/MTT-S Int. Microw. Symp.*, 2020, pp. 1283–1286.
- [28] X. Xie *et al.*, "Photonic microwave signals with zeptosecond-level absolute timing noise," *Nat. Photon.*, vol. 11, pp. 44–47, 2017.
- [29] A. Diakonov and M. Horowitz, "Generation of ultra-low jitter radio frequency phase pulses by a phase-locked oscillator," *Opt. Lett.*, vol. 46, no. 19, pp. 5047–5050, Oct. 2021.
- [30] J. Meier, A. Misra, S. Preußler, and T. Schneider, "Orthogonal full-field optical sampling," *IEEE Photon. J.*, vol. 11, no. 2, pp. 1–9, Apr. 2019.
- [31] A. Misra, J. Meier, S. Preußler, K. Singh, and T. Schneider, "Agnostic sampling transceiver," *Opt. Exp.*, vol. 29, no. 10, pp. 14828–14840, May 2021.
- [32] *IEEE Standard for Terminology and Test Methods for Analog-to-Digital Converters*, IEEE Standard 1241-2010 (Revision of IEEE Std 1241-2000), pp. 1–139, 2011.
- [33] P. O. Weigel *et al.*, "Bonded thin film lithium niobate modulator on a silicon photonics platform exceeding 100 GHz 3-dB electrical modulation bandwidth," *Opt. Exp.*, vol. 26, no. 18, pp. 23728–23739, Sep. 2018.
- [34] S. Hara *et al.*, "300-GHz CMOS transceiver for terahertz wireless communication," in *Proc. Asia-Pacific Microw. Conf.*, 2018, pp. 429–431.
- [35] K. K. O. *et al.*, "Opening terahertz for everyday applications," *IEEE Commun. Mag.*, vol. 57, no. 8, pp. 70–76, Aug. 2019.
- [36] X. Wu and H. K. Tsang, "Flat-top frequency comb generation with silicon microring modulator and filter," in *Proc. Conf. Lasers Electro- Opt.*, 2017, pp. 1/2.
- [37] I. Demirtzioglou *et al.*, "Frequency comb generation in a silicon ring resonator modulator," *Opt. Exp.*, vol. 26, no. 2, pp. 790–796, Jan. 2018.